Centimeter-Sized Aplanatic Hybrid Diffractive-Refractive Lens

Jian-Guan Hua, Zhi-Yong Hu, Si-Jia Xu, Zhen-Nan Tian, Yan-Hao Yu, Qi-Dai Chen, and Hong-Bo Sun, *Fellow, IEEE*

***Abstract*— The design and the fabrication of a hybrid diffractive-refractive lens (HDRL) by the femtosecond laser direct writing technique at 343-nm wavelength are demonstrated. The diffractive part is a 10-mm-diameter aplanatic element inside a Z-cut sapphire wafer. The refractive part is a spherical planoconvex lens with a 9.3-mm radius of curvature. These two parts are jointly combined to constitute a diffractive-refractive singlet. The hybrid singlet realizes aplanatic action for the aspherical lens, which reduces the focal spot size of the spherical lens by 1/4. The modulation transfer function of the hybrid singlet shows a better imaging resolution performance than that of the single spherical lens. The diffractive elements inside the spherical lens also were made and not only further improve thermal stability of the optical system but also reduce the volume and weight. This HDRL can find important applications in diffractive reflective hybrid optics, super-resolution imaging, and integrated optics.**

***Index Terms*— Femtosecond laser, hybrid diffractive-refractive lens, Aplanatism, imaging resolution.**

I. Introduction

THE modern tendency in the development of optics encompasses miniaturization, integration and high precision [1]–[4]. The traditional optical system is mainly designed on the principle of reflection and refraction utilizing refractors, prisms and reflectors. To achieve a better optical performance, many optical elements are combined together, and the result is a large volume and high cost per system, as well as inefficient use of light. In contrast, the hybrid diffractive-refractive optical system includes not only traditional elements but also diffractive optical elements (DOEs). Such system makes use of two properties of light in propagation—refraction and diffraction—which consist of unique chromatic dispersion, good thermal properties, monochromatic aberration correction capabilities and wave surface correction capability as compare to pure diffractive optical system [5]. For optical design, the hybrid optical system can not only improve the flexibility of the design but also break through many of the limitations in traditional optical systems [6], [7]. Consequently, compared with the traditional optical system, the hybrid diffractive-refractive optical system shows many advantages by improving system image quality, reducing volume, and lowering costs.

In recent years, buried optical elements (BOEs) have drawn much attention in scientific research and technology applications due to their considerable advantages [8]–[10]. Compared with the surface relief DOEs, BOEs are strongly resistant to friction and dust. Meanwhile, because of the ease of integration, BOEs are of great potential value to the field of integrated optics. Currently, buried DOEs combined with a traditional lens have been demonstrated. Here, we put forward a design where DOEs are inside a lens. In appearance, such a hybrid diffractive-refractive lens (HDRL) is no different from a single lens but can achieve a better flexibility in design and optical performance compared with diffractive lens. As a mature material processing technology, fs-laser [10], [11] direct writing (FsLDW) is a high-precision and true three-dimensional (3D) technique that has been widely applied for micro-optical elements, micromechanics and microelectronics [12]–[17]. Fs-laser can be focused beneath the surface inside transparent materials. Compared with other micromachining techniques, FsLDW has a unique capability to inscribe BOEs. When the focal spot of a fs-laser with the appropriate energy is scanned inside material, controlled changes in refractive index occurs [8]. The phase delay for the light propagating through the inscribed regions will take place. For this study we used the earlier established conditions of laser structuring of sapphire at UV 343 nm wavelength when inscribed regions have low scattering and refractive index change of 7.5×10^{-3} were obtained [18]. A higher efficiency of the diffractive element is achieved by varying the number of layers processed to achieve the designed phase delay. The short wavelength was important for a controlled definition of axial extent of the focus via two-photon absorption avoiding filamentation when longer pulses are used and Bessel beam like formation can occur [19], [20].

Optical performance of a lens is pinned to a small focal point required for better resolution or higher intensity. In a common optical system, surfaces of lenses are planes and spheres because such surfaces are easy to process and test. However, a single spherical lens cannot focus light beams to the smallest possible focus due to a large spherical aberration (SA). Using an aspherical lens can reduce the SA to some extent, but machining of aspheric lenses is more complex and costly. The aplanatic 2-level zone plate has been fabricated by FsLDW [10], but its narrowband working wavelength and low diffraction efficiency limit its application. The HDRL can improve the diffraction efficiency and the potential

Manuscript received July 2, 2018; revised October 24, 2018; accepted November 1, 2018. Date of publication November 9, 2018; date of current version December 20, 2018. This work was supported by National Key Research and Development Program of China and National Natural Science Foundation of China (NSFC) under Grants #2017YFB1104600, #61825502, #61805098, #61590930, and #61805100.

J.-G. Hua, Z.-Y. Hu, S.-J. Xu, Z.-N. Tian, Y.-H. Yu, and Q.-D. Chen are with the State Key Laboratory of Integrated Optoelectronics, College of Electronic Science and Engineering, Jilin University, Changchun 130012, China (e-mail: chenqd@jlu.edu.cn).

H.-B. Sun is with the State Key Laboratory of Integrated Optoelectronics, College of Electronic Science and Engineering, Jilin University, Changchun 130012, China, and also with the State Key Laboratory of Precision Measurement Technology and Instruments, Department of Precision Instrument, Tsinghua University, Beijing 100084, China (e-mail: hbsun@tsinghua.edu.cn).

Color versions of one or more of the figures in this letter are available online at http://ieeexplore.ieee.org.

Digital Object Identifier 10.1109/LPT.2018.2880013

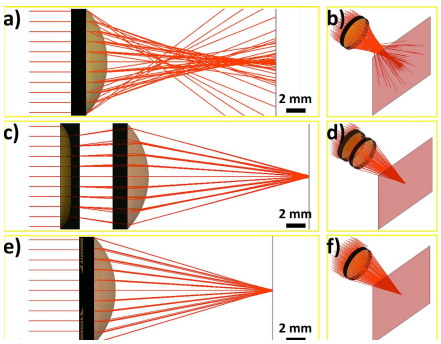

Fig. 1. Focusing simulated diagram of the spherical lens (a, b), the aplanatic battery of lenses (c, d) and the aplanatic HDRL (e, f) based on the ray tracing method. (a) (c) and (e): front views. (b) (d) and (f): oblique views.

of achromatism. To remove the SA of a spherical lens, refraction and diffraction are combined to process a diffractive optical lens on the spherical lens. In this work, reduction of unwanted SA was compensated by design of DOE. FsLDW was used to fabricate the BOEs inside the Z-cut sapphire crystal, to decrease the SA of the spherical lens. Also, a direct inscription of BOE inside a spherical lens was achieved.

II. Model and Experiments

In an optical system, when the aperture is large enough to exceed the paraxial condition, the light beams originating at different radial distances from the optical axis will not be brought together to a single focus by a lens. This defines the SA which is inherent for the spherical lens. When a parallel homochromatic wave passes through a spherical lens (12.7 mm in diameter, 9.17 mm in curvature radius and 4.3 mm in thickness), the ray-tracing of simulated optical path is shown in Fig. 1(a). The light rays near the optical axis (paraxial rays) would approximately gather in one point. However, the side off-axis rays converge on different points. Figure 1(b) shows the distribution of the focal spot affected by SA. The SA of the convex lens is negative, while that of the concave lens is positive; hence, the SA is compensated via a combination of multiple lenses. As is shown in Fig. 1(c), an aspheric concave lens is added to match the convex lens and the rays near and far from the axis are focused to a single focus (Fig. 1(d)). Such solution, however, leads to a bulky setup. In addition to augmented cost of such system it is less energy efficient due to multiple reflections. We design a BOE by quantizing phase profile of a concave lens into a multi-level element for fabrication by FsLDW. Such hybrid element can realize an aplanatic action of a single spherical lens (Fig. 1(e-f)).

First, the geometric ray tracing theory was used to optimize the SA of the hybrid lens. The optimum concave phase distribution of the diffractive element was calculated based on the software's iterative optimization algorithm. The phase distribution of the optimized element was obtained by formula $\Phi = 1.521629\rho^4 + 9.772811 \times 10^{-3}\rho^6 + 1.204454 \times 10^{-5}\rho^8$, where ρ is the distance from the optical axis. The gradual phase curve can reduce the processing accuracy requirements compared the single aplanatic diffractive element [10]. Thus, it was quantized to obtain a 4-level diffractive element for higher diffraction efficiency. The diffractive element was fabricated as separate SA compensator inside a Z-cut sapphire. High Abbe number of sapphire in visible spectral range brings extra merit for the compound optics for broad spectral range. Sapphire is also praised for its high chemical and thermal stability, high hardness. It is extremely difficult for traditional processing techniques to realize a high-precision fabrication of sapphire, while the fs-laser can machine almost any material due to its extremely high peak intensity. Importantly for discussed application, fs-laser pulses can be focused inside sapphire, and by controlling an exposure appropriately, the refractive index at the focal volume can be changed without surface ablation. FsLDW was applied to fabricate an optical element inside sapphire by scanning the fs-laser focus. Here, a near-ultraviolet radiation of fs-laser (Light-Conversion Pharos) at wavelength of $\lambda = 343$nm, a repetition rate of 200 kHz and a pulse duration of 300 fs was utilized. Circularly polarized light was used to reduce possibility of nanograting formation [21] and experiments were carried out at the close-to-the-threshold conditions for optically recognizable modification. Laser beam was passed through a 3^X beam expander and was focused by a reflecting objective (Thorlabs LMM-40X-P01 with numerical aperture NA = 0.5). The shorter wavelength of the laser allowed for higher machining accuracy, that is, the single-point machining precision can reach sub-diffractional resolution due to the threshold effect in modification of ~200 nm (the diameter at the focus is d = 1.22λ/NA=0.84 μm). The sample to be processed is fixed on a high-speed 3D air-bearing rotary stage (Aerotech ABRT-150) with a large stroke length and good stability. The maximum processing length can reach up to 10 cm required for accurate fabrication of macroscopic optical elements designed in this study. The average laser power measured before the objective was 50 mW, and the rotational speed of the air-bearing rotary stage was 2 mm/s. The fourth-order zone plate consists of three layers (i.e., the 2π phase is accumulated in four λ/4 steps), and fs-laser scanned in layer-by-layer. The three-layer element not only ensures that the larger phase delay of 1.5π to achieve near-ideal diffraction efficiency of 71%, but also guarantees to some extent the higher efficiency of processing large size devices. The bottom layer was recorded first at a depth of 100 μm. Next, the air-bearing rotary stage was moved 15 μm along the Z direction to scan the second layer, and the third layer was scanned last. The diameter of the aplanatic diffractive element fabricated was 10 mm. Such large-size diffractive structure takes approximately 6 h for the processing of each layer. The 3D air-bearing rotary stage allowed comparatively fast FsLDW fabrication with high accuracy and precision.

To visualize the BOE, the conventional fourth-order zone plate was characterized by fluorescence confocal microscopy (FCFM) to visualize the structure. Figure 2(a) shows the FCFM photographs of the entire structure of the fourth-order zone plate obtained with 4^X objective lens. Images in Fig. 2(b-d) were obtained by sequentially focusing on the first layer, second layer and third layer of the zone plate with 20^X objective lens. Specifically, when the microscope was focused on the first layer, as shown in Fig. 2(b), the zone plate rings were the narrowest. When the microscope was focused on the second layer (Fig. 2(c)) and the zone plate rings were wider. Finally, on the third layer (Fig. 2(d)), the zone plate rings were the widest. By using this imaging method, it is possible to perfectly present the structural topography of different layers of the buried multi-stage zone plate.

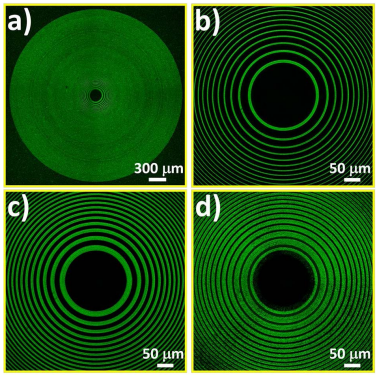

Fig. 2. (a) The overall optical microscope image of the zone plate. (b-d) FCFM images of the first, second and third layers, respectively.

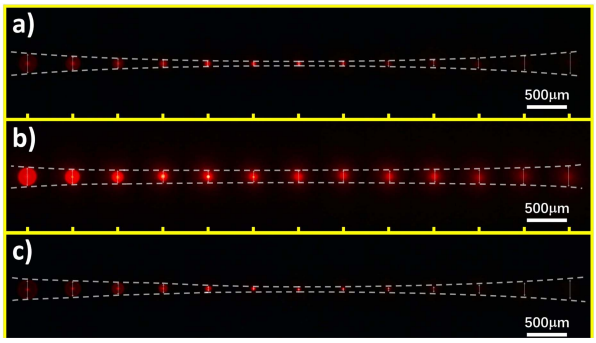

Fig. 3. The images of light spots taken at each 200 μm shift along the optical axis, (a): the HDRL, (b): the spherical lens (c): the aspherical lens.

III. Results and Discussion

For testing optical properties of HDRL, a 633-nm-wavelength laser beam was passed through a diffusively scattering glass to obtain an incoherent light. Then, the light beam was expanded to approximate the plane wave. Then, light was sent through the lens and imaged by a charge-coupled device (CCD). Tests were carried on HDRL and single spherical lens and the results of which are shown in Fig. 3(a) and (b), respectively. For better comparison, optical tests were also carried out for an aspherical lens of the same size and focus, as shown in Fig. 3(c). CCD was placed in the focal position of the lens and took pictures of the light spot. By attenuating the incident light, the light intensity could be reduced to ensure that the energy per pixel of the focus would not saturate CCD. By moving CCD along optical axis, size evolution was taken in 200 μm steps. Divergence of the focus is visualized. From the focal appearance marked by the yellow circle, the focus of the single spherical lens presents a disc of blur with a relatively large spot size, while the spot of the HDRL was comparable with that of the aspherical lens.

To measure the size of the focal spot accurately, the intensity distribution in the focal plane was plotted. Figure 4(a) shows the focal cross section for the HDRL, Fig. 4(b) - for the spherical lens, and Fig. 4(c) for the commercial aspherical lens. The black and red lines describe the horizontal and vertical cross sections, respectively. It is easy to see that the spot sizes of the HDRL and the aspherical lens are both considerably smaller than that of the spherical lens. The waist sizes of those three kinds of lenses were, 56.5 μm, 188.4 μm and 57.9 μm, respectively. Recognizable focal spots of these

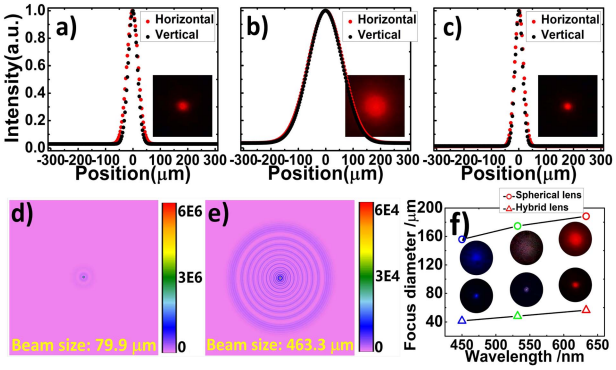

Fig. 4. (a-c) The energy distribution curves of the focal spots of the HDRL, the spherical lens and the aspherical lens. (d-e) The simulated focused light field topography images of the HDRL and the spherical lens. (f) The focus sizes of the hybrid lens and the spherical lens with different wavelengths.

lenses were 168.1 μm, 646.4 μm and 150.7 μm, respectively. The HDRL shortens the focal spot of the spherical lens to 1/4 of its size, and meanwhile, the spherical lens achieves the aplanatic focusing of the aspherical lens. In addition, based on the theory of light-field tracing, the focused light-field topography images of the hybrid lens and the spherical lens were simulated by the light-field simulation software Virtual Lab Fusion (LightTrans, Germany), as shown in Fig. 4(d-e). Based on the simulation results, the focal spot size of the diffractive hybrid lens was 79.9 μm, and that of the spherical lens was 463.3 μm. In the experiment, the focal spot size of the hybrid lens is slightly larger than the theoretical value, which may be due to a deviation of the phase delay of the processed diffractive element. At the same time, the focal spot size of the hybrid lens and the spherical lens at the wavelengths of 450 nm and 532 nm has been measured. As shown in Fig. 4(f), the focal size enlarges slightly for longer wavelength. The results also verify that the hybrid lens has an aplanatic effect at other wavelengths.

Apart from the focusing property, the imaging resolution is also an important optical property of the lens [10]. To better demonstrate the performance of the HDRL, the modulation transfer function (MTF) of the HDRL was characterized, which is identified as a scientific optical evaluation standard. Based on the resolving power test target, which encompasses periodic lines of different widths in horizontal and vertical directions, the imaging resolution of the hybrid lens was measured. The width range of the periodic lines was approximately 10-40 μm, and the length was 350 μm. The numbers of lines of different widths within the length of 1 mm were correspondingly defined as spatial frequencies. A 633 nm laser was shone on the target and imaging by HDRL was recorded by CCD. Shown in Fig. 5(c-d) are the imaging pictures for the HDRL and spherical lens. As the number of line pairs increased, the hybrid lens maintained a high imaging definition, but for the spherical lens, the imaging photos become blurred and it was very hard to distinguish periodic fringes. The MTF formula is given by

$$\mathrm{M} = (I_{max} - I_{min})/(I_{max} + I_{min})$$

where I_{max} and I_{min} are the maximum illuminance and minimum illuminance, respectively. Based on the formula, the MTFs of the hybrid lens and the spherical lens with

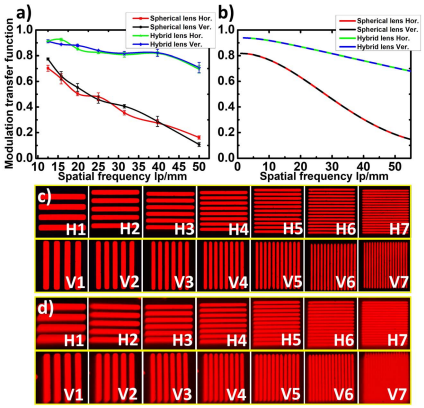

Fig. 5. (a) Experimental MTF curves of the hybrid lens and the spherical lens. (b) Theoretical MTF curves of the hybrid lens and the spherical lens. (c-d) The resolution chart images of the hybrid lens and the spherical lens.

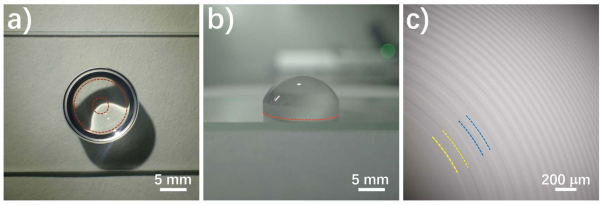

Fig. 6. (a-b) Physical photographs of the HDRL, (a): top views. (b): front view. (c) The photomicrograph of the diffractive element in the lens.

different line pairs were obtained. The experimental MTF curves are shown in Fig. 5(a). One can see that with an increase of the spatial frequency, the MTF of the hybrid lens reduces slowly, while the MTF of the spherical lens reduces rapidly. When the spatial frequency is 50, the MTF of the hybrid lens can still be maintained above 0.7. Compared to the spherical lens, the imaging resolution property of the hybrid lens was considerably better. The Virtual Lab Fusion theoretical simulation curves of the MTFs for the hybrid and spherical lens are in good agreement with the experimental test results, as shown in Fig. 5(b). By the experiment and the theoretical simulation of MTFs, a better imaging resolution of the hybrid lens has been verified.

Finally, a 10-mm-diameter diffractive element was fabricated inside a spherical lens that had a diameter of 12.7 mm and a focal length of 15 mm. The integrated HDRL is virtually indistinguishable in appearance from a single refractive lens, whose front view and lateral view are shown in Fig. 6(a-b). The buried structure is marked in the red frame and the photomicrograph is shown in Fig. 6(c). The annulus marked by the yellow lines was the zone machined by fs-laser, and the zone marked by the blue lines wasn't machined. This design not only improves a design freedom required for thermal stability of multi-component lenses but also reduces the size and weight of the hybrid system.

IV. Conclusions

The aplanatic HDRL fabricated by FsLDW at UV wavelength could achieve excellent aplanatic focusing and imaging performance compared with spherical lens. Moreover, the BOEs can be fabricated inside the refractive element by FsLDW, to achieve the integration of the refractive and diffractive elements. This work has not only paved the way for the fabrication of HDRL using FsLDW but also has made it possible to realize high performance of diffractive-refractive hybrid optical system. The optical element with the buried diffractive structure holds great promise for applications in the fields of integrated optics, optical communication and sensing in harsh environments.

References

[1] K. M. Davis, K. Miura, N. Sugimoto, and K. Hirao, "Writing waveguides in glass with a femtosecond laser," *Opt. Lett.*, vol. 21, no. 21, pp. 1729–1731, Nov. 1996.

[2] Y. Cheng *et al.*, "Three-dimensional micro-optical components embedded in photosensitive glass by a femtosecond laser," *Opt. Lett.*, vol. 28, no. 13, pp. 1144–1146, Jul. 2003.

[3] J. T. Lin *et al.*, "Low-threshold whispering-gallery-mode microlasers fabricated in a Nd: Glass substrate by three-dimensional femtosecond laser micromachining," *Opt. Lett.*, vol. 38, no. 9, pp. 1458–1460, May 2013.

[4] S. Juodkazis, V. Mizeikis, and H. Misawa, "Three-dimensional microfabrication of materials by femtosecond lasers for photonics applications," *J. Appl. Phys.*, vol. 106, no. 5, p. 8, Sep. 2009.

[5] T. Stone and N. George, "Hybrid diffractive-refractive lenses and achromats," *Appl. Opt.*, vol. 27, no. 14, pp. 2960–2971, Jul. 1988.

[6] S. Thiele, A. Seifert, and A. M. Herkommer, "Wave-optical design of a combined refractive-diffractive varifocal lens," *Opt. Express*, vol. 22, no. 11, pp. 13343–13350, Jun. 2014.

[7] H. Liu, Y. Yan, D. Yi, and G. Jin, "Theories for the design of a hybrid refractive-diffractive superresolution lens with high numerical aperture," *J. Opt. Soc. Amer. A*, vol. 20, no. 5, pp. 913–924, May 2003.

[8] M. Beresna, M. Gecevičius, and P. G. Kazansky, "Ultrafast laser direct writing and nanostructuring in transparent materials," *Adv. Opt. Photon.*, vol. 6, no. 3, pp. 293–339, Sep. 2014.

[9] S. Juodkazis *et al.*, "Laser induced memory bits in photorefractive $LiNbO_3$ and $LiTaO_3$," *Appl. Phys. A, Solids Surf.*, vol. 93, no. 1, pp. 129–133, Oct. 2008.

[10] Z. N. Tian *et al.*, "Aplanatic zone plate embedded in sapphire," *IEEE Photon. Technol. Lett.*, vol. 30, no. 6, pp. 509–512, Mar. 15, 2018.

[11] A. Stone *et al.*, "Femtosecond laser-writing of 3D crystal architecture in glass: Growth dynamics and morphological control," *Mater. Des.*, vol. 146, pp. 228–238, May 2018.

[12] L. L. Gao *et al.*, "Optical-induced electrical current in diamond switched by femtosecond-attosecond laser pulses by *ab initio* simulations," *J. Phys. D, Appl. Phys.*, vol. 49, no. 2, Jan. 2016.

[13] L. Wang *et al.*, "Plasmonic nano-printing: Large-area nanoscale energy deposition for efficient surface texturing," *Light Sci. Appl.*, vol. 6, p. e17112, Dec. 2017.

[14] F. Chen *et al.*, "Maskless fabrication of concave microlens arrays on silica glasses by a femtosecond-laser-enhanced local wet etching method," *Opt. Express*, vol. 18, no. 19, pp. 20334–20343, Sep. 2010.

[15] K. Sugioka and Y. Cheng, "Ultrafast lasers–reliable tools for advanced materials processing," *Light Sci. Appl.*, vol. 3, p. e149, Apr. 2014.

[16] M. Sakakura *et al.*, "Fabrication of three-dimensional 1×4 splitter waveguides inside a glass substrate with spatially phase modulated laser beam," *Opt. Express*, vol. 18, no. 12, p. 12136–12143, Jun. 2010.

[17] J. Lv *et al.*, "Femtosecond laser written optical waveguides in z-cut $MgO:LiNbO_3$ crystal: Fabrication and optical damage investigation," *Opt. Mater.*, vol. 57, pp. 169–173, Jul. 2016.

[18] Q. K. Li *et al.*, "Multilevel phase-type diffractive lens embedded in sapphire," *Opt. Lett.*, vol. 42, no. 19, pp. 3832–3835, Oct. 2017.

[19] E. Gaizauskas, E. Vanagas, V. Jarutis, S. Juodkazis, V. Mizeikis, and H. Misawa, "Discrete damage traces from filamentation of Gauss-Bessel pulses," *Opt. Lett.*, vol. 31, no. 1, pp. 80–82, Jan. 2006.

[20] S. Juodkazis *et al.*, "Application of femtosecond laser pulses for microfabrication of transparent media," *Appl. Surf. Sci.*, vol. 197, pp. 705–709, 2002.

[21] R. Buividas, S. Rekštytė, M. Malinauskas, and S. Juodkazis, "Nanogroove and 3D fabrication by controlled avalanche using femtosecond laser pulses," *Opt. Mater. Express*, vol. 3, no. 10, pp. 1674–1686, 2013.